

Electronic and magnetic properties of $\text{K}_2\text{CuP}_2\text{O}_7$: A model $S = \frac{1}{2}$ Heisenberg chain system

R. Nath, Deepa Kasinathan, H. Rosner,* M. Baenitz, and C. Geibel

Max Planck Institut für Chemische Physik fester Stoffe, Nöthnitzer Strasse 40, 01187 Dresden, Germany

(Received 7 January 2008; revised manuscript received 19 March 2008; published 30 April 2008)

The electronic and magnetic properties of $\text{K}_2\text{CuP}_2\text{O}_7$ were investigated by means of susceptibility, specific heat and ^{31}P nuclear magnetic resonance (NMR) measurements and by local density approximation (LDA) band structure calculations. The temperature dependence of the NMR shift $K(T)$ is well described by the $S = \frac{1}{2}$ Heisenberg antiferromagnetic chain (HAF) model with nearest neighbor exchange $J_1 \approx (141 \pm 5)$ K. The corresponding mapping of an LDA-derived tight-binding model leads to $J_1^{\text{LDA}} \approx 196$ K. The spin lattice relaxation rate $1/T_1$ decreases with temperature below 300 K but becomes nearly temperature independent between 30 and 2 K, as theoretically expected for an $S = \frac{1}{2}$ HAF chain. None of the investigated properties give any evidence for long range magnetic order above 2 K, which is in agreement with the results of the band structure calculation, which yield extremely weak exchange to the next nearest neighbor and a very small and frustrated interchain exchange. Thus, $\text{K}_2\text{CuP}_2\text{O}_7$ seems to be a better realization of a nearest neighbor $S = \frac{1}{2}$ HAF chain than the compounds reported so far.

DOI: [10.1103/PhysRevB.77.134451](https://doi.org/10.1103/PhysRevB.77.134451)

PACS number(s): 75.10.Pq, 75.40.Cx, 76.60.Cq

I. INTRODUCTION

One-dimensional (1D) spin systems have attracted considerable attention because of their intriguing ground states where quantum fluctuations play a crucial role. Much excitement in their magnetism has been caused by the theoretical prediction that the integer-spin chains have an energy gap in the excitation spectrum,¹ while the half-integer spin chains have a gapless excitation spectrum.^{2,3} In particular, 1D $S = \frac{1}{2}$ Heisenberg antiferromagnetic (HAF) systems are interesting since enhanced quantum fluctuations due to reduced dimensionality and low spin value impede long range magnetic order (LRO). In the past decade, theoretical studies on these systems have achieved a remarkable progress but real material realizations for such compounds are limited to date.

The $S = \frac{1}{2}$ chains formed via direct linkage of CuO_4 units can be grouped into two categories: in one group, the chains are formed by edge-sharing CuO_4 units, while in the other compound family, they are built from corner-sharing CuO_4 units. CuGeO_3 and Li_2CuO_2 belong to the former category,^{4,5} where the nearest neighbor (NN) interaction J_1 and the next-nearest neighbor (NNN) interaction J_2 have comparable strength ($\frac{|J_2|}{|J_1|} \approx 1$), thereby leading to a strong frustration within the chain. In such a scenario, various ground states are possible. On the contrary, in Sr_2CuO_3 which has corner shared CuO_4 units $\frac{|J_2|}{|J_1|} \approx \frac{1}{20}$, which greatly reduces the in-chain frustration.⁶⁻⁸ With $J_1 \gg T_N$, Sr_2CuO_3 is a better quasi-1D $S = \frac{1}{2}$ chain system than CuGeO_3 and Li_2CuO_2 . Recently, another system, $\text{Sr}_2\text{Cu}(\text{PO}_4)_2$, containing isolated CuO_4 units (neither edge nor corner shared) was reported to have $\frac{J_2}{J_1} \approx \frac{1}{700}$ and a much reduced T_N of 85 mK.⁹⁻¹² The presence of interchain coupling (ic) normally provides LRO, while frustrating ic reduces the tendency to LRO. Along with $J_1 \gg T_N$, the presence of frustration between the chains strongly influences the 1D nature of this system, making it a nearly perfect realization for the 1D NN only HAF chain model. Unfortunately, the sample quality was not very good, thereby reducing the chains to a finite length. The analytical

solution by Bethe ansatz² provides a clear picture of the magnetic (thermodynamic) properties of a very good 1D material. Thus, deviations from these predictions can be assigned to other degrees of freedom [anisotropy, Dzyaloshinskii–Moriya (DM), and other spin-spin interactions], allowing us to analyze their influence on the ground state behavior. Therefore, strong interest still prevails in the experimental community to find possible ways to synthesize a system which keeps the in-chain geometry of $\text{Sr}_2\text{Cu}(\text{PO}_4)_2$, but with a smaller interchain coupling, which is still frustrating, along with an improved sample quality.

Formally, $\text{K}_2\text{CuP}_2\text{O}_7$ belongs to the family of $M_2\text{CuP}_2\text{O}_7$ ($M = \text{Li, Na, K}$) compounds, although the arrangement of the magnetic CuO_4 building blocks is modified within the family. The magnetic properties of $\text{Na}_2\text{CuP}_2\text{O}_7$ and $\text{Li}_2\text{CuP}_2\text{O}_7$ were reported earlier.^{13,14} $\text{Na}_2\text{CuP}_2\text{O}_7$ and $\text{Li}_2\text{CuP}_2\text{O}_7$ both have an in-chain exchange coupling J_1 of about 28 K and they undergo magnetic ordering at around 5 K. Unlike the other members of this family, our experiments reveal that $\text{K}_2\text{CuP}_2\text{O}_7$ shows a much stronger in-chain exchange interaction ($J_1 \approx 141$ K) but no ordering down to 2 K. Due to such a wide $T_N - J_1$ temperature range, it can be considered as a very good candidate on which to test the theoretical predictions of both static and dynamic properties of an 1D HAF model.

In this paper, we present susceptibility, specific heat, ^{31}P NMR results and first principles band structure calculations on $\text{K}_2\text{CuP}_2\text{O}_7$ in order to shed light on the 1D character of the system. The paper is organized as follows: In Secs. II and III, we describe the structural aspects, measurement procedures, and the theoretical methodology. In Sec. IV, we present the experimental results followed by the electronic structure analysis. In Sec. V, we address the issues concerning the almost ideal 1D nature of this compound inferred from the ^{31}P NMR and band structure calculations. In Sec. VI we give a short summary and conclusions.

II. STRUCTURE

$\text{K}_2\text{CuP}_2\text{O}_7$ crystallizes in an orthorhombic unit cell with space group $Pbnm$. The reported lattice constants are a

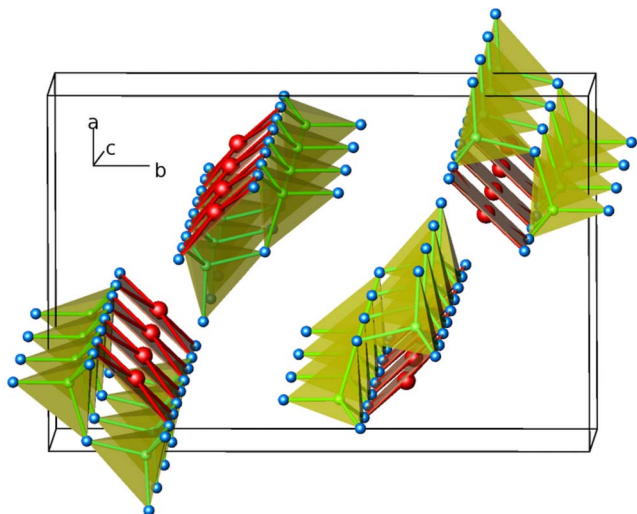


FIG. 1. (Color online) $K_2CuP_2O_7$ crystal structure. The CuO_4 square planes (red) share their edges with the PO_4 tetrahedra (green) to form $[Cu(PO_4)_2]_\infty$ linear chains propagating along the c direction. The potassium cations reside in between the chains (not shown here).

$=9.509 \text{ \AA}$, $b=14.389 \text{ \AA}$, and $c=5.276 \text{ \AA}$.¹⁵ In the crystal structure, isolated quasiplanar CuO_4 units are linked by PO_4 tetrahedra, forming $[Cu(PO_4)_2]_\infty$ chains propagating along the crystallographic c direction. A scheme of the basic building blocks of the crystal is shown in Fig. 1. The superexchange between Cu^{2+} ions in $K_2CuP_2O_7$ will be similar to that of edge sharing CuO_4 chains with every second CuO_4 unit cutoff. In such a situation, J_2 (NNN) in the edge shared system will become J_1 (NN) in our system (of the order of ≈ 100 K), and J_2 in our system will be comparable to J_4 (fourth neighbor interaction along the chain) in the edge shared system, which is known to be quite negligible. The chains are well separated from each other since the potassium cations, K^{1+} reside in between the chains. The inter-chain interactions are expected to be very weak, unlike $Sr_2Cu(PO_4)_2$ since the chains do not lie in the same plane. Magnetic properties of this compound have not been reported yet.

III. METHODS

A. Experiment

Polycrystalline $K_2CuP_2O_7$ was prepared by solid state reaction techniques using K_2CO_3 (99.9% pure), CuO (99.99% pure), and $NH_4H_2PO_4$ (99.9% pure) as starting materials. The stoichiometric mixtures were fired at $640 \text{ }^\circ\text{C}$ for 60 h in air, with one intermediate grinding. The samples were characterized using a STOE powder diffractometer with a Cu target ($\lambda_{av}=1.54182 \text{ \AA}$). The powder pattern evidenced single phase material. The lattice parameters obtained using a least-squares fit procedure are $a=9.541(3) \text{ \AA}$, $b=14.407(5) \text{ \AA}$, and $c=5.253(1) \text{ \AA}$, which are close to the previously reported values.¹⁵

Magnetization (M) data were measured as a function of temperature T between 2 and 400 K in fields up to 5 T on

powder samples in a commercial (Quantum design) superconducting quantum interference device (superconducting quantum interference device) magnetometer. Specific heat $C_p(T)$ measurements were performed on a pressed pellet using relaxation method in a commercial PPMS (physical property measurement system) equipment (Quantum design). NMR measurements were carried out using pulsed NMR techniques on ^{31}P nuclei (nuclear spin $I=\frac{1}{2}$ and gyromagnetic ratio $\gamma/2\pi=17.237 \text{ MHz/T}$) at 70 MHz, which corresponds to an applied field of about 40.6 kOe. Spectra were obtained by Fourier transform of the NMR echo signal using a $\pi/2$ pulse with width of about $2 \mu\text{s}$. The NMR shift $K(T)=[\nu(T)-\nu_{ref}]/\nu_{ref}$ was determined by measuring the resonance frequency of the sample $[\nu(T)]$ with respect to a standard H_3PO_4 solution (resonance frequency ν_{ref}). The spin-lattice relaxation rate ($1/T_1$) was measured by the saturation recovery method. Our attempt to see the ^{63}Cu signal was not successful due to the fast relaxation at the magnetic site.

B. Theory

The band structure calculations presented here utilized version 5.00-18 of the full-potential local orbital band structure^{16,17} (FPLO) method. The structure, lattice constants, and atomic positions have been taken from experiment.¹⁵ The core states have been treated fully relativistically, while the semicore (K: $3s3p$, Cu: $3s3p$, and P: $2s2p$) and the valence states (K: $3d4s4p$, Cu: $3d4s4p$, P: $3s3p3d$, and O: $2s2p3d$) are treated scalar relativistically. The extent of the valence basis functions was optimized with respect to the total energy.¹⁸ The Brillouin zone sampling was based on 216 k points in the irreducible wedge. We have used the Perdew and Wang¹⁹ flavor of the exchange and correlation potential when performing the calculations within the local density approximation (LDA).

IV. RESULTS

A. Susceptibility and specific heat

Bulk magnetic susceptibility $\chi(T)(=M/H)$ was measured as a function of temperature in an applied field of 5 kOe (Fig. 2). As shown in Fig. 2, the sample exhibits a shoulder at about 100 K, suggesting a maximum in this temperature range, which is a hallmark of low-dimensional magnetic interactions. With further decreasing temperature, $\chi(T)$ increases again in a Curie–Weiss manner. Common sources for such an increase are the presence of paramagnetic impurities or finite length chains due to disorder. However, an intrinsic Curie like tail is expected in a quasi-1D $S=\frac{1}{2}$ chain, if DM interaction and/or a staggered g -factor anisotropy are present.^{20,21} Among the $3d$ systems, Cu benzoate²² and pyrimidine Cu dinitrate²³ are well known examples. No obvious features associated with LRO were observed for $1.8 \leq T \leq 400$ K.

In order to fit the bulk susceptibility data, we decomposed χ into

$$\chi = \chi_0 + \frac{C_{imp}}{T + \theta_{imp}} + \chi_{spin}(T), \quad (1)$$

where the first term χ_0 is temperature independent and accounts for the diamagnetism of the core electron shells and

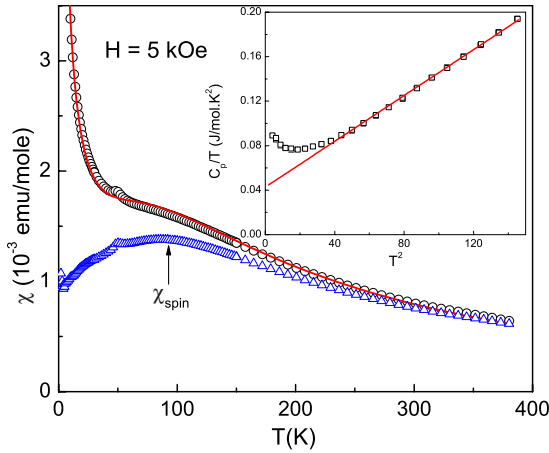


FIG. 2. (Color online) Magnetic susceptibility (M/H) vs temperature T for $\text{K}_2\text{CuP}_2\text{O}_7$ (open circles) in an applied field of 5 kOe. The solid line is best fit of the data to Eq. (1). Spin susceptibility χ_{spin} is plotted (open triangles) after subtracting the Curie contribution. In the inset, C_p/T is plotted as a function of T^2 for the low temperatures. The solid line represents a linear fit.

Van-Vleck paramagnetism of the open shells of the Cu^{2+} ions. The second term $\frac{C_{imp}}{T+\theta_{imp}}$ is the low T Curie-Weiss contribution due to paramagnetic species in the sample. $\chi_{spin}(T)$ is the spin susceptibility for a uniform $S=\frac{1}{2}$ 1D HAF system, which is known quite precisely over the whole measured temperature range. We took Johnston's expression²⁴ valid for $5 \times 10^{-25} \leq \frac{T}{J_1} \leq 5$.

A fit of Eq. (1) to the experimental data leads to the parameters $\chi_0 \approx 2.7 \times 10^{-4}$ emu/mole, $C_{imp} \approx 0.026$ emu K/mole, $\theta_{imp} \approx 0.7$ K, and $J_1 \approx 145$ K. Because of large Curie tail, such a fit is unstable at high temperatures. Therefore, we reduced the number of fitting parameters by fixing $g=2.2$ (obtained from NMR shift analysis).²⁵ The value of χ_0 is comparable to that found in Sr_2CuO_3 .⁷ The Curie contribution present in the sample would correspond to a defect spin concentration of 6.9% assuming defect spin $S=\frac{1}{2}$. Alternatively, it would correspond to the contribution expected for finite chains with a length of ≈ 15 spins according to the calculation of Schmidt *et al.*²⁶ We add in Fig. 2 a plot of χ_{spin} as a function of temperature after subtracting the Curie contribution. Now, a pronounced broad maximum around 100 K is well resolved. The small peak at 50 K corresponds to a parasitic contribution of adsorbed oxygen. Unfortunately, we failed to improve the quality of the sample, since further annealing (in flowing Ar or vacuum) did not lead to any noticeable change in the x-ray diffraction pattern.

The information about the lattice dimensionality can be obtained from the low temperature specific heat $C_p(T)$. For a $S=\frac{1}{2}$ chain, one expects a linear term, whereas for a square lattice, one expects a leading quadratic term in the absence of excitation gap. In the C_p/T vs T^2 plot (shown in the inset of Fig. 2) in the temperature range $5 \leq T \leq 12$ K, one can clearly see that the plot follows a straight line over a considerable temperature range. This indicates that $C_p(T)$ is a sum of a linear and a cubic contribution. Since the cubic term corresponds to the expected contribution of the phonons, this demonstrate that the leading term of the magnetic con-

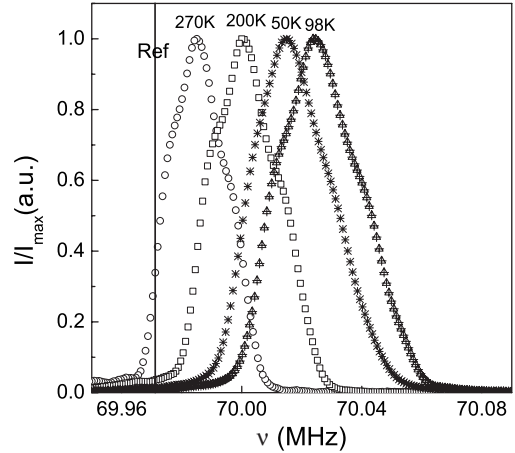


FIG. 3. ^{31}P NMR spectra at different temperatures T . The solid line represents the nonmagnetic ^{31}P reference.

tribution is linear in T . For an $S=\frac{1}{2}$ HAF chain, theoretical calculations^{24,27} predict for low temperatures ($T < 0.2J_1$); $\frac{C_p}{T} = \frac{2R}{3J_1} = \gamma_{theor}$. With $J_1 \approx 141$ K obtained from the NMR shift $K(T)$ analysis (presented later), this corresponds to a value $\gamma_{theor} \approx 0.04$ J/K² mole. Fitting the measured data in the range $5 \leq T \leq 12$ K, we obtained $\gamma_{expt} \approx 0.042$ J/K² mole. The value of γ_{expt} is close to the value predicted theoretically. This strongly supports the quasi-1D nature of the spin system in $\text{K}_2\text{CuP}_2\text{O}_7$. No other anomaly was observed down to 2 K in $C_p(T)$, suggesting the absence of magnetic order. Below 5 K, our experimental data deviates upward from the straight line fit (inset, Fig. 2). This is likely related to the contributions of paramagnetic impurities and of chain ends, which should follow a $C \approx A/T^2$ behavior.

B. ^{31}P NMR

Although our analysis of the susceptibility and specific heat suggests the presence of a $S=\frac{1}{2}$ 1D HAF system, the evidence is only of preliminary nature because of the large Curie tail in $\chi(T)$ at low T . In order to gain a more reliable insight into this system, we turned our attention towards NMR results. NMR has the advantage to be much less sensitive to contribution of defects or impurities because usually only the nucleus on an undistorted site contributes to the narrow NMR line. As shown in the crystal structures (Fig. 1), $\text{K}_2\text{CuP}_2\text{O}_7$ has two inequivalent ^{31}P sites, which are coupled inductively to Cu^{2+} ions in the chain. Therefore, ^{31}P NMR can probe accurately the low-lying excitations in the spin chain. Our ^{31}P NMR spectra consist of a single spectral line as is expected for $I=\frac{1}{2}$ nuclei (Fig. 3). Although there are two inequivalent ^{31}P sites present in the crystal structure, a single resonance line implies that both the ^{31}P sites in this compound are nearly identical. With decreasing temperature, the NMR line shifts away from the Larmor frequency, paramagnetically broadens but the overall line shape remain same down to 2 K. The asymmetric shape of the spectra corresponds to a powder pattern due to an asymmetric hyperfine coupling.

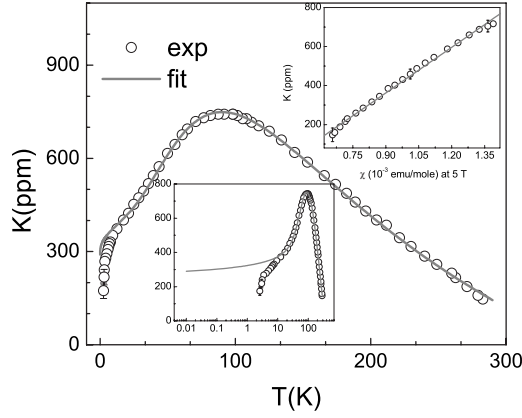


FIG. 4. Temperature dependence of the ^{31}P NMR shift $K(T)$ of $\text{K}_2\text{CuP}_2\text{O}_7$. The solid line is the fit with Eq. (2) in the temperature range $9 \leq T \leq 300$ K and further extrapolated down to 0 K. The lower inset shows K vs T on a logarithmic temperature scale for improved visualization of the low- T data. In the upper inset, K vs χ is plotted with temperature as an implicit parameter and the solid line is the linear fit.

The temperature dependence of the NMR shift K is shown in Fig. 4. With decreasing temperature $K(T)$ paramagnetically increases, then passes through a broad maximum at 110 K, which is an indicative of short-range correlations, and decreases again smoothly toward low temperatures. Below $\frac{T}{J_1} \approx 0.028$, $K(T)$ shows a much steeper decrease toward zero. As mentioned before, the NMR has an advantage over bulk susceptibility. One accurately measures the χ_{spin} by NMR shift without suffering from the contribution from the free spins and extrinsic foreign phases, which limits the accuracy of the bulk susceptibility measurements. Therefore, it is more reliable to extract the magnetic parameters from the temperature dependence of the NMR shift rather than from the bulk susceptibility. The conventional scheme of correlating $K(T)$ and $\chi(T)$ is to plot, K vs χ_{spin} with T as an implicit parameter. Then, the slope yields the average hyperfine coupling A_{hf} between the ^{31}P nucleus and the two nearest-neighbor Cu^{2+} ions. In the case of $\text{K}_2\text{CuP}_2\text{O}_7$, because of the low T Curie tail in $\chi(T)$, this $K(T)$ vs $\chi(T)$ plot shows a straight line only for $T > 110$ K (see upper inset of Fig. 4). Nevertheless, we can estimate $A_{hf} \approx 4400 \pm 400 \text{ Oe} / \mu_B$, which is about two times stronger than in other phosphate systems.^{9,28} We then determine J_1 and g by fitting the temperature dependence of K to the following equation:

$$K = K_0 + \left(\frac{A_{hf}}{N\mu_B} \right) \chi_{spin}(T, J_1), \quad (2)$$

where K_0 is the temperature independent chemical shift. As shown in Fig. 4, the $K(T)$ data fit rather well to Eq. (2) in the temperature range $9 \leq T \leq 300$ K. By using $A_{hf} \approx 4400 \text{ Oe} / \mu_B$ (obtained from the K vs χ analysis), we obtained $K_0 \approx -890$ ppm, $J_1 \approx (141 \pm 5)$ K, and $g \approx 2.2$. Below about 8 K, $K(T)$ show a significant deviation from the fit (see lower inset of Fig. 4), which shall be discussed later.

The temperature dependence of ^{31}P $1/T_1$ is presented in Fig. 5. For a $I = \frac{1}{2}$ nucleus the recovery of the longitudinal

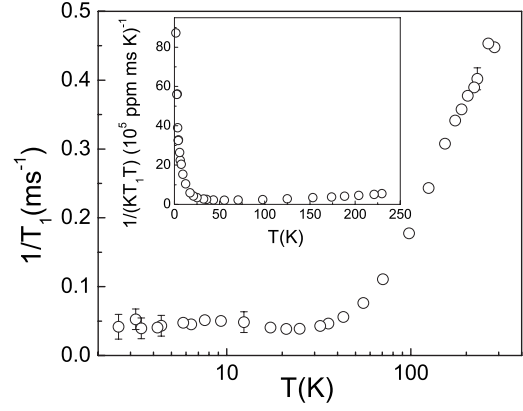


FIG. 5. Spin-lattice relaxation rate $1/T_1$ vs temperature T measured at 70 MHz. In the inset, $1/(KT_1T)$ is shown all over the temperature range.

magnetization is expected to follow a single exponential behavior. In the experiment, we indeed observed single exponential behavior down to 30 K, while below 30 K, it fitted nicely to the stretch exponential with a reduced exponent. We did not observe any anomaly or divergence in $1/T_1(T)$ down to 2 K, which indicates the absence of magnetic ordering. For $2 \leq T \leq 30$ K, $1/T_1$ almost remains constant, while for $T \geq 30$ K, it strongly increases with temperature. A slight shoulder is visible in the plot $1/T_1$ versus $\ln T$ around 180 K, i.e., just above J_1 , suggesting a regime crossover in this temperature range.

C. First principles and tight binding

Collected in Fig. 6 are the nonmagnetic band structure and the density of states (DOS). The antibonding band is made from a half-filled $\text{Cu } 3d_{x^2-y^2} - \text{O } 2p_\sigma$ molecular orbital belonging to the CuO_4 plaquettes. The band structure shows strong dispersion of about 55 meV parallel to the chain direction ΓZ and XA but is nearly dispersionless within the crystallographic a - b plane (i.e., perpendicular to the direction of the chains), indicative of the strong 1D character in this system. Within LDA, we get a metallic behavior, though the system is an insulator, suggested by its blue color.¹⁴ This is a well known artifact of LDA wherein the effect of strong correlations is under estimated. Including the strong correlations for the $\text{Cu } 3d$ states will open up the insulating gap. This can be achieved via two possible ways: (a) performing an LDA+ U calculation self-consistently, (b) mapping the results from LDA first to a tight-binding model (TBM). The TBM is then mapped on to a Hubbard model, and subsequently to a Heisenberg model because the system belongs to the strong correlation limit $U \gg t$ (t is the leading transfer integral) at half filling.

In order to better understand the microscopic magnetic interactions in this system, we have followed the second option mentioned above. First, we have considered the TBM,

$$H = \sum_{\langle i,j \rangle, \sigma} t_{ij} C_{i,\sigma}^\dagger C_{j,\sigma} + \sum_i \epsilon_i \hat{n}_i, \quad (3)$$

where t_{ij} are the hopping integrals, $C_{i,\sigma}^\dagger C_{j,\sigma}$ are annihilation and creation operators. From the LDA band structure, we

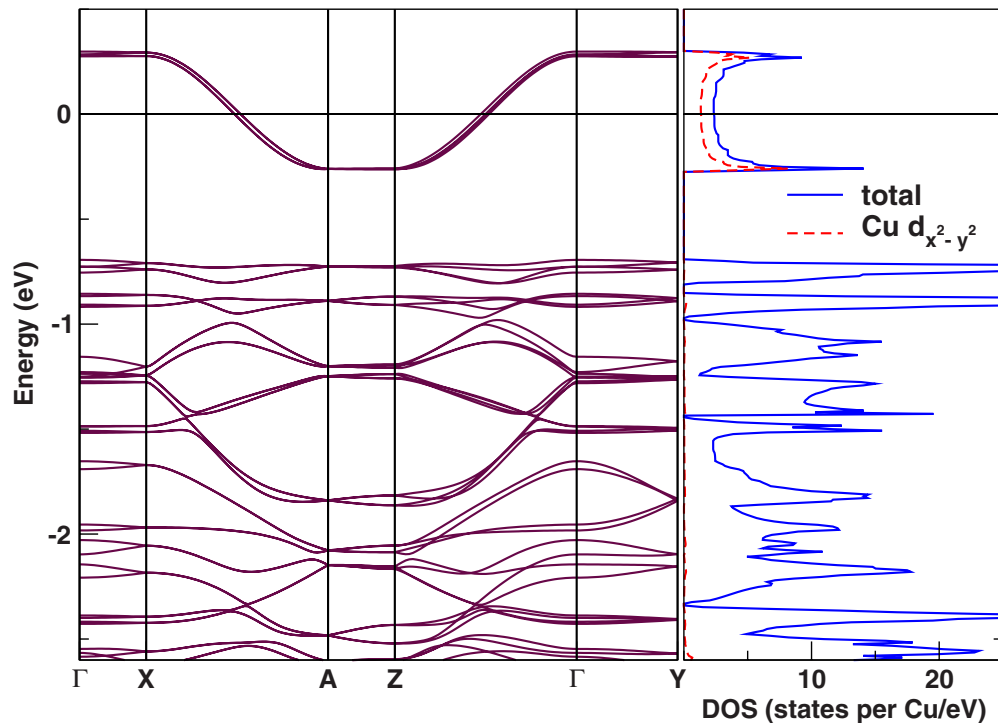


FIG. 6. (Color online) Left panel: The nonmagnetic band structure of $\text{K}_2\text{CuP}_2\text{O}_7$ along the high-symmetry directions of a standard orthorhombic unit cell. X - A and Z - Γ denote the directions along the chain (i.e., along crystallographic c axis), wherein the dispersion is the largest, while the perpendicular-to-chain directions Γ - X and Γ - Y are rather nondispersive. There are four copper sites per unit cell leading to four half-filled metallic bands at the Fermi level, well separated from all other bands. Right panel: The total DOS for $\text{K}_2\text{CuP}_2\text{O}_7$ along with the Cu $d_{x^2-y^2}$ orbitally resolved contributions. A comparison to the band structure clearly elucidates that the half-filled metallic band at the Fermi level is primarily from Cu $d_{x^2-y^2}$ and O p_σ molecular plaquette orbital.

have extracted only the four antibonding Cu $3d_{x^2-y^2}$ bands and performed a fit to the TBM. All the hopping paths considered in our model are shown in Fig. 7. The hopping integrals were calculated using the steepest descent method. The resulting parameters, which provided the best fit to the LDA band structure (Fig. 8), are collected in Table I. The strength of the NN hopping t_1 along the chain is 2 orders of magnitude larger than all the other hoppings, attributing the strong one dimensionality to the interaction of the plaquettes along the chain. The individual exchange constants are calculated by using $J_{ij}^{AFM} = 4t_{ij}^2/U_{eff}$. The value of U_{eff} for $\text{K}_2\text{CuP}_2\text{O}_7$ is set to 4.5 eV, the same as the choice in related 1D compounds $(\text{Sr},\text{Ba})_2\text{Cu}(\text{PO}_4)_2$.¹¹ The total exchange constant is given by $J^{total} = J^{AFM} + J^{FM}$. The J values collected in Table I are indicative of the J^{AFM} only. In $\text{K}_2\text{CuP}_2\text{O}_7$, the CuO_4 plaquettes are separated from each other, with no corner-or edge-sharing oxygens. The absence of direct connections between the plaquettes largely suppresses ferromagnetic interactions between the copper sites. The strength of the FM interactions was shown to be very small in the related systems $(\text{Sr},\text{Ba})_2\text{Cu}(\text{PO}_4)_2$,¹¹ and this result should equally hold for our system.

V. DISCUSSION

The quality of the fit for the NMR shift supports the presence of an $S = \frac{1}{2}$ HAF chain. The exchange coupling ($J_1 \approx 141$ K) is comparable to that found in other phosphates⁹

and in nice agreement with the effective NN superexchange constant, $J_1^{LDA} = 196$ K obtained from the TBM. The slight overestimation may stem from the fact that U_{eff} is not exactly known, along with some FM contributions. Such an overestimation of J by LDA is well known and is also observed in $(\text{Sr},\text{Ba})_2\text{Cu}(\text{PO}_4)_2$.¹¹ The NNN superexchange

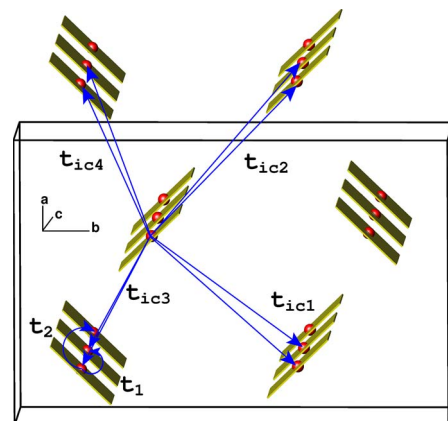


FIG. 7. (Color online) The various hopping paths considered in our tight-binding model to reproduce the half-filled metallic LDA band are shown here. We have considered two hoppings along the chain (t_1, t_2) and four interchain hoppings ($t_{1c1}, t_{1c2}, t_{1c3}, t_{1c4}$) in all. Starting from one chain, Cu in the next neighbor chain are shifted by half of the in-chain Cu-Cu distance, leading to two identical interactions to two Cu spins in each adjacent chains.

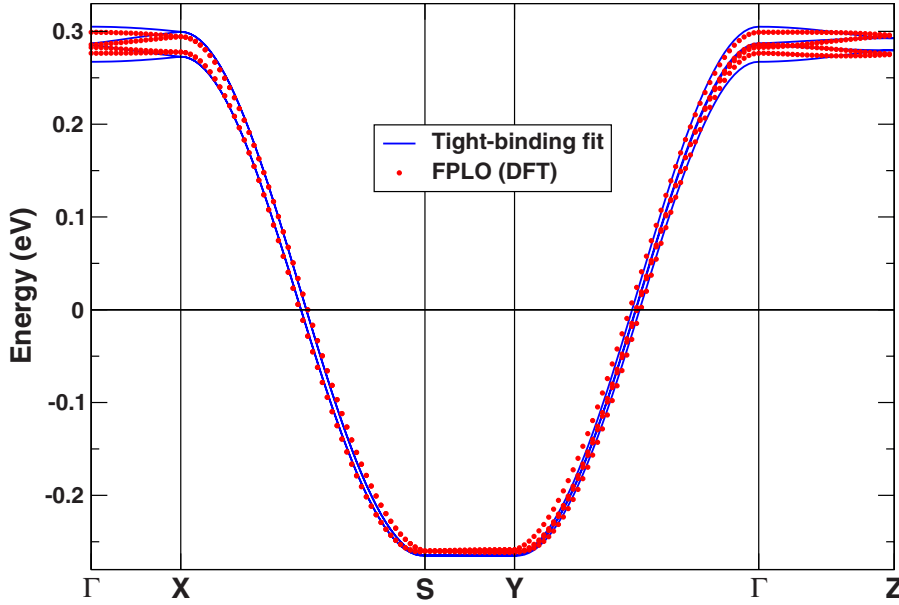


FIG. 8. (Color online) The superposition of the total band structure from the FPLO density functional theory (DFT) calculations along with the calculated eigenvalues from the four-site one-band TBM. The TBM fit is quite consistent with the DFT results.

constant $J_2^{LDA} = 0.04$ K is extremely small, so frustration coupling, if any, should be negligible. The ratio of first and second neighbor in-chain coupling is $J_1^{LDA}/J_2^{LDA} \geq 5000$, the largest found in $S = \frac{1}{2}$ chain system. The ratio of in chain to the strongest (frustrating) interchain coupling is $J_1^{LDA}/J_{ic4}^{LDA} \geq 1000$, which is 2 orders of magnitude larger than in $\text{Sr}_2\text{Cu}(\text{PO}_4)_2$ ($J_1^{LDA}/J_{ic}^{LDA} \sim 70$) (Ref. 11) and 1 order of magnitude larger than Sr_2CuO_3 ($J_1^{LDA}/J_{ic}^{LDA} \sim 500$) (Refs. 8 and 29) and making $\text{K}_2\text{CuP}_2\text{O}_7$ an even better realization of 1D HAF behavior than the Sr analog. We have estimated the Néel temperature of $\text{K}_2\text{CuP}_2\text{O}_7$ (T_N^K) by adapting a simple mean field approximation^{8,30} and comparing it to the Sr analogue (T_N^{Sr}). Assuming that the anisotropy are the same in both compounds, we can write according to Ref. 8

$$\frac{T_N^K}{T_N^{\text{Sr}}} \approx \frac{\sqrt{J_1^K J_{ic}^K}}{\sqrt{J_1^{\text{Sr}} J_{ic}^{\text{Sr}}}}, \quad (4)$$

where, $T_N^{\text{Sr}} \approx 85$ mK.¹⁰ Since the incompleteness in the mapping should be the same for both the compounds, we can directly compare the values of T_N . We have used $J_1^{\text{Sr}} = 187$ K, $J_{ic}^{\text{Sr}} = 0.23$ K (geometrical average of the 2 inter-chain exchanges), $J_1^K = 196$ K, and $J_{ic}^K = \sqrt[4]{J_{ic1}^{LDA} J_{ic2}^{LDA} J_{ic3}^{LDA} J_{ic4}^{LDA}} = 0.037$ K. By plugging these values in the above equation, we get $T_N^K \approx 37$ mK, which is a factor of 2 smaller than the Sr analog. This value sets an upper bound because the value of J_{ic} is calculated by using a mean-field approximation. The

absence of anomalies in $K(T)$, $1/T_1(T)$, and the invariant spectral shape down to low temperatures rules out the possibility of LRO down to 2 K, which is consistent with the theoretical prediction of an extremely low T_N . In $\text{K}_2\text{CuP}_2\text{O}_7$, each CuO_4 plaquettes in one chain has two identical neighbors in each adjacent chains, with the same exchange interactions. For a strong in-chain AFM exchange, this leads to a complete frustration of the interchain interactions. Quantum fluctuations are therefore enhanced here which suppresses T_N to lower values.

For a 1D $S = \frac{1}{2}$ HAF, theoretical calculations predict a weak logarithmic decrease of $\chi(T)$ upon approaching $T = 0$ K (see Fig. 4). The lower inset of Fig. 4 clearly shows that the decrease we observe in $K(T)$ of $\text{K}_2\text{CuP}_2\text{O}_7$ is much more pronounced. The susceptibility of a 1D $S = \frac{1}{2}$ HAF at $T = 0$ is exactly known,²⁴ $\chi(T=0) = \frac{g^2 \mu_B^2}{k_B(J_1) \pi^2}$. Then, $K(T)$ at zero temperature can be written as $K_{\text{theor}}(T=0) = K_0 + [\frac{A_{hf} g^2 \mu_B^2}{k_B(J_1)}] \times \frac{1}{\pi^2}$. Using the parameters (K_0 , A_{hf} , g , and J_1) determined from our $K(T)$ analysis, $K_{\text{theor}}(T=0)$ was calculated to be 260 ppm. However, our experimental value at 2 K is much lower, only 180 ppm, and $K(T)$ is still decreasing steeply with T at this temperature. Thus, at the quantitative level, the theoretically predicted logarithmic term fails to describe our experimentally observed decrease. A similar feature has been experimentally found in ^{17}O NMR on Sr_2CuO_3 below $T/J_1 \approx 0.015$ (Ref. 31) and ^{31}P NMR on $(\text{Sr}, \text{Ba})_2\text{Cu}(\text{PO}_4)_2$ below $T/J_1 \approx 0.003$.⁹ In both the cases, it is argued that the decrease

TABLE I. Hopping parameters (in meV) and the corresponding exchange constants J (in K) from an effective one-band tight-binding model. The hopping paths used are indicated in Fig. 7.

	t_1	t_2	t_{ic1}	t_{ic2}	t_{ic3}	t_{ic4}
meV	138	2	2	2	0.8	4
	J_1^{LDA}	J_2^{LDA}	J_{ic1}^{LDA}	J_{ic2}^{LDA}	J_{ic3}^{LDA}	J_{ic4}^{LDA}
K	196	0.04	0.04	0.04	0.007	0.16

is unrelated to the onset magnetic order or a spin-Peierls transition. In $\text{K}_2\text{CuP}_2\text{O}_7$, we neither saw any indication of ordering in $1/T_1(T)$ nor in $C_p(T)$. Similarly, there is no signature of exponential decrease (or singlet ground state) observed in $1/T_1(T)$ as is expected for a spin-Peierls transition. One possibility to account for this drop in $K(T)$ is the presence of DM interaction arising from the fact that in $\text{K}_2\text{CuP}_2\text{O}_7$, there is no center of inversion symmetry-relating two neighboring copper atoms along the chain. In the presence of DM interaction, application of a magnetic field parallel to the DM vector opens a gap Δ in the magnetic excitation spectra. Since in a first approximation Δ increases with B to the power $2/3$, it shall not be visible in the $B=0$ specific heat data or the low field susceptibility shown in Fig. 2. However, further experiments are needed to confirm or discard this explanation.

In NMR valuable information on the dynamic of low-energy spin excitations can be gained from the analysis of the temperature dependence of nuclear spin-lattice relaxation rates. Therefore, it is essential to analyze $1/T_1(T)$ carefully, which yields information about the imaginary part of the dynamic susceptibility $\chi(\mathbf{q}, \omega)$. Thus, $1/T_1$ should include contributions from both the uniform ($q=0$) and staggered ($q=\pm\frac{\pi}{a}$) spin fluctuations. A theoretical analysis by Sachdev³² shows that the staggered component is dominant at low temperatures ($T \ll J_1$). Indeed, the uniform component leads to $1/T_1 \propto T$, while the staggered component gives $1/T_1 = \text{constant}$. Monte Carlo calculations by Sandvik supported the validity of these results over an appropriate temperature range.³³ As shown in Fig. 5, our experimentally observed constant $1/T_1$ at low temperatures ($2 \leq T \leq 30$ K) suggests the dominance of staggered fluctuations at low temperatures. The ^{31}P form factor for such systems is defined in Ref. 9. Since ^{31}P is symmetrically located between the Cu ions, the fluctuations are expected to be filtered out provided the hyperfine couplings are equal. Moreover, in this case, we still have a significant remnant contribution from $q = \pm\pi/a$, which plays a dominant role at low temperatures. The possible origin of the remnant staggered fluctuations could be the unequal hyperfine couplings. In fact, such features have been previously observed in a few other 1D $S=\frac{1}{2}$ HAF systems, where $J_1 \gg T_N$.^{9,13,31,34,35} The strong increase of $1/T_1$ with T above 30 K could be attributed to the uniform fluctuations. When the dominant contribution is from $q=0$, then one expects a constant $1/(KT_1T)$. In $\text{K}_2\text{CuP}_2\text{O}_7$, for $T \geq 30$ K, we rather observe a weak temperature dependency (inset of Fig. 5), which might be due to some remanent contributions from the staggered fluctuations and/or some additional relaxation mechanisms. This weak temperature dependence as well as the reduction of the slope in the plot $1/T_1$ versus T above 180 K might be related to spin diffusion as observed in $\alpha\text{-VO}(\text{PO}_3)_2$ above J_1 .³⁶

The relaxation rate due to staggered fluctuations can be calculated following the prescription of Barzykin.³⁷ For the purpose of comparison of theory with experiment, he defined the normalized dimensionless NMR spin-lattice relaxation

rate at low temperature $(1/T_1)_{\text{norm}} = \frac{\hbar J_1}{A_{\text{hf}}^2 T_1} \approx 0.3$, where A_{hf} is $A_{\text{hf}}(2h\gamma/2\pi)$. Assuming the fluctuations to be correlated because of the exchange J_1 along the chains, $1/T_1$ can be written as $1/T_1 = \frac{0.3}{\hbar J_1/A_{\text{hf}}^2}$. By using this expression, $(1/T_1)$ at the ^{31}P site was calculated to be about 129 s^{-1} , whereas our experimental value is 50 s^{-1} in the $2 \leq T \leq 30$ K range. The experimental value is about two times smaller than the theoretical value, likely due to the effect of the geometrical form factor. Further on a weak logarithmic increase in $1/T_1$ is theoretically expected at low temperatures.³⁷ In the present case, our measurements were not done down to low enough temperatures to rise this contribution above our experimental error.

VI. CONCLUSION

In conclusion, our experimental and theoretical studies of $\text{K}_2\text{CuP}_2\text{O}_7$ demonstrate that this compound presents a very uniform and strongly 1D $S=\frac{1}{2}$ HAF chain system. Our NMR, specific heat, and susceptibility measurements show good agreement with theoretical predictions for a 1D $S=\frac{1}{2}$ HAF chain. Thus, the temperature dependence of the NMR shift K can be fitted in good agreement with model calculations giving $J_1 \approx 141 \pm 5$ K. A calculation of the exchange interactions using a TBM fitted to the results of *ab initio* LDA band structure calculations, subsequently mapped onto a Heisenberg model, leads to a quite similar value of $J_1 \approx 190$ K and evidences extremely weak NNN interactions as well as extremely weak and “frustrated” interchain exchange of the order of $J^{ic} \sim 0.1$ K, which is in contrast to $\text{Sr}_2\text{Cu}(\text{PO}_4)_2$ with $J^{ic} \sim 9$ K (Ref. 11) and to Sr_2CuO_3 “nonfrustrated” $J^{ic} \sim 10$ K.⁸ The absence of any evidence for magnetic order above 2 K in the experimental data confirms the weakness of the interchain exchanges. By using the TBM results, a rough estimate of the Néel temperature results in a value of $T_N \sim 37$ mK only. $\text{K}_2\text{CuP}_2\text{O}_7$ has the smallest in-chain as well as frustrating smallest interchain exchanges, which do not suppress quantum fluctuations, thereby making this system an even better example of a 1D $S=\frac{1}{2}$ HAF system than the compounds reported so far.

We further studied the magnetic fluctuations by analyzing the temperature dependence of $1/T_1$. At low temperatures $1/T_1$ remains constant, which is in reasonable agreement with Sachdev’s predictions for 1D $S=\frac{1}{2}$ HAF system where relaxation is dominated by $q = \pm\pi/a$ at low T . Below 5 K, we obtained a decrease of the NMR shift K , which is more pronounced than that expected for a 1D $S=\frac{1}{2}$ HAF. Its origin is not clear yet but might be due to DM interactions.

ACKNOWLEDGMENTS

We thank A. V. Mahajan and F. Haarmann for their critical suggestions on NMR. We would like to acknowledge Alois Loidl for some preliminary NMR measurements done in his group laboratory. D.K. and H.R. acknowledge financial support from the “Emmy-Noether-program” of the DFG.

*rosner@cpfs.mpg.de

- ¹F. D. M. Haldane, Phys. Rev. Lett. **50**, 1153 (1983).
- ²H. A. Bethe, Z. Phys. **71**, 205 (1931).
- ³E. Lieb, T. D. Schultz, and D. C. Mattis, Ann. Phys. **16**, 407 (1961).
- ⁴L. F. Mattheiss, Phys. Rev. B **49**, 14050 (1994).
- ⁵R. Neudert, H. Rosner, S.-L. Drechsler, M. Kielwein, M. Sing, Z. Hu, M. Knupfer, M. S. Golden, J. Fink, N. Nucker, M. Merz, S. Schuppler, N. Motoyama, H. Eisaki, S. Uchida, M. Domke, and G. Kaindl, Phys. Rev. B **60**, 13413 (1999).
- ⁶T. Ami, M. K. Crawford, R. L. Harlow, Z. R. Wang, D. C. Johnston, Q. Huang, and R. W. Erwin, Phys. Rev. B **51**, 5994 (1995).
- ⁷N. Motoyama, H. Eisaki, and S. Uchida, Phys. Rev. Lett. **76**, 3212 (1996).
- ⁸H. Rosner, H. Eschrig, R. Hayn, S.-L. Drechsler, and J. Malek, Phys. Rev. B **56**, 3402 (1997).
- ⁹R. Nath, A. V. Mahajan, N. Buttgen, C. Kegler, and A. Loidl, and J. Bobroff, Phys. Rev. B **71**, 174436 (2005).
- ¹⁰Alexei A. Belik, S. Uji, T. Terashima, and E. Takayama, J. Solid State Chem. **178**, 3461 (2005).
- ¹¹M. D. Johannes, J. Richter, S.-L. Drechsler, and H. Rosner, Phys. Rev. B **74**, 174435 (2006).
- ¹²S. S. Salunke, M. A. H. Ahsan, R. Nath, A. V. Mahajan, and I. Dasgupta, Phys. Rev. B **76**, 085104 (2007).
- ¹³R. Nath, A. V. Mahajan, N. Buttgen, C. Kegler, J. Hemberger, and A. Loidl, J. Phys. Condens. Matter **18**, 4285 (2006).
- ¹⁴L. Alexander *et al.* (private communication)
- ¹⁵A. ElMaadi, A. Boukhari, and E. M. Holt, J. Alloys Compd. **223**, 13 (1995).
- ¹⁶K. Koepernik and H. Eschrig, Phys. Rev. B **59**, 1743 (1999).
- ¹⁷I. Opahle, K. Koepernik, and H. Eschrig, Phys. Rev. B **60**, 14035 (1999).
- ¹⁸H. Eschrig, *Optimized LCAO Method* (Springer-Verlag, Berlin, 1989).
- ¹⁹J. P. Perdew and Y. Wang, Phys. Rev. B **45**, 13244 (1992).
- ²⁰M. Oshikawa and I. Affleck, Phys. Rev. Lett. **79**, 2883 (1997).
- ²¹I. Affleck and M. Oshikawa, Phys. Rev. B **60**, 1038 (1999).
- ²²D. C. Dender, D. Davidovic, Daniel H. Reich, Collin Broholm, Kim Lefmann, and G. Aeppli, Phys. Rev. B **53**, 2583 (1996).
- ²³R. Feyrerherm, A. Abens, D. Günther, T. Ishida, M. Meissner, M. Meschke, T. Nogami, and M. Steiner, J. Phys. Condens. Matter **12**, 8495 (2000).
- ²⁴D. C. Johnston, R. K. Kremer, M. Troyer, X. Wang, A. Klümper, S. L. Bud'ko, A. F. Panchula, and P. C. Canfield, Phys. Rev. B **61**, 9558 (2000).
- ²⁵Using g as a free parameter results in a reduced value of about 1.8. Nevertheless, in either case it does not lead to a significant change in the value of J_{\perp} (~ 130 K).
- ²⁶B. Schmidt, V. Yushankhai, L. Siurakshina, and P. Thalmeier, Eur. Phys. J. B **32**, 43 (2003).
- ²⁷A. Klumper, Eur. Phys. J. B **5**, 677 (1998).
- ²⁸A. V. Mahajan, R. Nath, N. Buttgen, C. Kegler, A. Loidl, and J. Bobroff, Physica B **378**, 1148 (2006).
- ²⁹Taking the measure of $J_{\perp}=190$ meV from the magnetic susceptibility experiment of Ref. 7 and the empirical $J_{\perp}=0.2$ meV, calculated from the ordering temperature $T_N=5$ K, using coupled quantum spin chain approach as in Ref. 8, we find $J_{\parallel}/J_{\perp} \sim 600$ still 1 order of magnitude smaller than $\text{K}_2\text{CuP}_2\text{O}_7$.
- ³⁰V. Yu. Irkhin and A. A. Katanin, Phys. Rev. B **61**, 6757 (2000).
- ³¹K. R. Thurber, A. W. Hunt, T. Imai, and F. C. Chou, Phys. Rev. Lett. **87**, 247202 (2001).
- ³²S. Sachdev, Phys. Rev. B **50**, 13006 (1994).
- ³³A. W. Sandvik, Phys. Rev. B **52**, R9831 (1995).
- ³⁴M. Takigawa, N. Motoyama, H. Eisaki, and S. Uchida, Phys. Rev. Lett. **76**, 4612 (1996).
- ³⁵M. Takigawa, O. A. Starykh, A. W. Sandvik, and R. R. P. Singh, Phys. Rev. B **56**, 13681 (1997).
- ³⁶J. Kikuchi, N. Kurata, K. Motoya, T. Yamauchi, and Y. Ueda, J. Phys. Soc. Jpn. **70**, 2765 (2001).
- ³⁷V. Barzykin, Phys. Rev. B **63**, 140412(R) (2001).